

Missing Thermal Energy of the Intracluster Medium

Niayesh Afshordi,^{1*} Yen-Ting Lin,^{2,3} Daisuke Nagai,⁴ and Alastair J. R. Sanderson⁵

¹*Institute for Theory and Computation, Harvard-Smithsonian Center for Astrophysics, MS-51, 60 Garden Street, Cambridge, MA 02138, USA*

²*Princeton University Observatory, Princeton University, Princeton, NJ 08544, USA*

³*Departamento de Astronomía y Astrofísica, Pontificia Universidad Católica de Chile*

⁴*Theoretical Astrophysics, California Institute of Technology, Mail Code 130-33, Pasadena, CA 91125, USA*

⁵*School of Physics and Astronomy, University of Birmingham, Edgbaston, Birmingham B15 2TT, UK*

25 October 2018

ABSTRACT

The Sunyaev-Zel'dovich (SZ) effect is a direct probe of thermal energy content of the Universe, induced in the cosmic microwave background (CMB) sky through scattering of CMB photons off hot electrons in the intracluster medium (ICM). We report a 9σ detection of the SZ signal in the CMB maps of Wilkinson Microwave Anisotropy Probe (WMAP) 3yr data, through study of a sample of 193 massive galaxy clusters with observed X-ray temperatures greater than 3 keV. For the first time, we make a model-independent measurement of the pressure profile in the outskirts of the ICM, and show that it closely follows the profiles obtained by X-ray observations and numerical simulations. We find that our measurements of the SZ effect would account for only half of the thermal energy of the cluster, if all the cluster baryons were in the hot ICM phase. Our measurements indicate that a significant fraction, $35\% \pm 8\%$, of baryonic mass are missing from the hot ICM, and thus must have cooled to form galaxies, intracluster stars, or an unknown cold phase of the ICM. There does not seem to be enough mass in the form of stars or cold gas in the cluster galaxies or intracluster space, signaling the need for a yet-unknown baryonic component (at 3σ level), or otherwise new astrophysical processes in the ICM.

1 INTRODUCTION

Galaxy clusters are remarkable laboratories for studying structure formation and cosmology. Thanks to their physical size of \sim Mpc, they can be easily resolved in different frequencies, ranging from radio, optical to X-rays, and thus any model for cluster physics can be independently tested against various observations. The simple model that is borne out of these studies can then be used as a standard candle/ruler that probes the geometry and dynamics of the Universe at cosmological redshifts (e.g., Borgani 2006).

However, the simple theoretical picture of cluster formation through gravitational collapse is complicated by other astrophysical processes such as shock-heating and radiative cooling of gas, star formation, energy feedback and chemical enrichment of the ICM by supernovae and accreting super-massive black holes. Most of our observational understanding of the intracluster medium (ICM) to date has come from the study of its diffuse X-ray emission, which has led to a multitude of theoretical investigations on the effects of gas cooling and heating of the ICM (see Voit 2005, for a review). Although modern high-resolution hydrodynamic simulations have enabled detailed theoretical modeling of cluster formation, the details of star formation or interactions with super-massive black holes are still far beyond the numerical resolution limit, and our understanding of details and relative importance of most of these processes still remain quite uncertain. Therefore, further observational stud-

ies of clusters in X-ray and other wavebands will continue to be the key in guiding physical modeling of cluster properties and formation.

The thermal Sunyaev Zel'dovich (SZ) effect is a unique observational probe of galaxy clusters detectable in radio and microwave frequencies. It is a spectral distortion in CMB spectrum caused by inverse-Compton scattering of CMB photons off hot electrons in the ICM (Sunyaev & Zel'dovich 1972; Birkinshaw 1999). As the number of photons does not change through scattering, the SZ effect causes a decrement (increment) in the intensity of CMB at low (high) frequencies. The effect has the unique property that its signal is independent of redshift, and it directly probes the ICM pressure, or thermal energy density. These features make the SZ effect a particularly unique and powerful observational tool for detecting clusters at cosmological redshifts ($z \gtrsim 0.5$) and hence a promising cosmological probe of dark energy (see Carlstrom et al. 2002, for a review).

Although various CMB experiments are now aiming at carrying out SZ cluster surveys, all-sky CMB surveys with sufficient resolution to detect many SZ clusters directly (such as *Planck*; Geisbuesch & Hobson 2006) are yet non-existent. The highest resolution all-sky map of the CMB sky has been recently released by the Wilkinson Microwave Anisotropy Probe (WMAP) group (Hinshaw et al. 2006). The WMAP maps alone do not show any significant signature of the SZ effect (Spergel et al. 2006). Al-

though the WMAP SZ signals of individual cluster have a low significance, it is possible to combine SZ signatures of many clusters to obtain constraints on the mean ICM properties. First efforts in this direction have been made through direct cross-correlation of galaxy/cluster surveys in optical/IR bands with the CMB temperature maps obtained by WMAP (Bennett et al. 2003a; Fosalba et al. 2003; Fosalba & Gaztañaga 2004; Myers et al. 2004; Afshordi et al. 2004). These measurements have led to $2-5\sigma$ detection of anti-correlation with different galaxy and cluster surveys, which is consistent with the expected SZ signal at WMAP frequencies (Afshordi et al. 2004; Hernández-Monteagudo & Rubiño-Martín 2004).

More optimal detection of SZ effect is possible via cross-correlation of the CMB maps with the temperature of the X-ray emitting ICM, since both the SZ and X-ray probe the same hot ICM. This was a primary motivation for our study of the WMAP 1st year data. In Afshordi, Lin & Sanderson (2005, ALS05 hereafter), we reported an 8σ detection of the SZ signal, through an optimized correlation of WMAP 1st year data release (Bennett et al. 2003b) with a catalog of X-ray clusters. Using a theoretically motivated ICM profile for the analysis, ALS05 have shown that the gas fraction in clusters is $\sim 30 - 40\%$ low compared to the universal baryon fraction of the Universe. If the clusters contain a representative mix of dark matter and baryons of the Universe (Evrard 1990; Metzler & Evrard 1994; Navarro et al. 1995; Lubin et al. 1996; Eke et al. 1998; Frenk et al. 1999; Mohr et al. 1999; Bialek et al. 2001; Kravtsov et al. 2005; Ettori et al. 2006; McCarthy et al. 2006), this number would be far too low to account for the expected baryon budgets in clusters, since the observed stellar and cold gas fraction is no larger than $\approx 10 - 15\%$ (Gonzalez et al. 2005; Lin & Mohr 2004). These results are in agreement with other SZ (LaRoque et al. 2006) and X-ray (Ettori 2003; Vikhlinin et al. 2006) studies. These results therefore indicate that the baryons are missing from the expected baryon budget of clusters.

Much larger discrepancies with X-ray observations have been reported in Lieu et al. (2006), who claim that the WMAP SZ signal for ROSAT X-ray clusters is a factor of ~ 4 smaller than the expectation from X-ray brightness profiles. However, in order to compare with WMAP maps, Lieu et al. (2006) extrapolate the β -model fits far beyond the region that is fit by X-ray data, suggesting that the reported discrepancy may simply be an artifact of this extrapolation, which is known to fail at large radii (e.g., Vikhlinin et al. 1999; Schmidt et al. 2004; Vikhlinin et al. 2006).

Given the importance of the problem, we repeat the measurements of ALS05 using the 3 year WMAP data in this paper. The improvements from the previous analyses are two-folds. First, the WMAP 3yr data release (Hinshaw et al. 2006) should provide a higher significance detection of the SZ signal, while still capturing large angle information that is missing from higher resolution interferometric experiments. Second, we devise a model-independent method to measure the mean ICM pressure profile from WMAP temperature maps for a catalog of X-ray clusters. The latter will help minimize the dependence on theoretical assumptions and associated systematic uncertainties, which often dominate systematic uncertainties in SZ analyses carried out us-

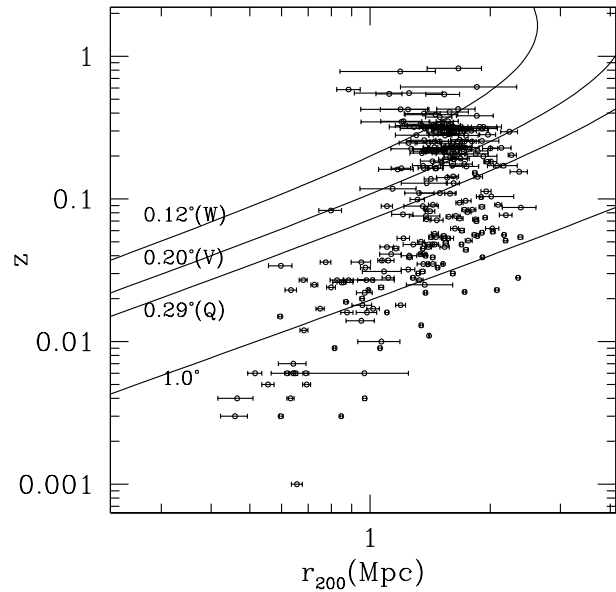


Figure 1. The distribution of cluster redshifts and virial radii (estimated from X-ray temperature; see Sec. 2.2). The three upper lines show the resolution of WMAP bands (associated with the radius of the disk with the same effective area as the detector beams; see Jarosik et al. 2006), while the lower line shows the physical radius of the 1 degree circle at the cluster redshift.

ing a cluster model (see e.g., ALS05; LaRoque et al. 2006). We then use this measurement to put constraints on the thermal energy and baryonic budget of the ICM.

The paper is organized as follows. In the next section we describe our methodology, including compilation of our X-ray cluster catalog, our method to extract the SZ signal from the CMB maps, and the hydrodynamic simulations that we compare to the data. Our main observational results are described in Sec. 3. In Sec. 4, we discuss the possible shortcomings, as well as the implications of our analysis, the most puzzling of which is a missing baryonic component of the ICM. Finally, Sec. 5 concludes the paper.

2 METHODOLOGY

2.1 X-ray cluster catalog

Our primary objective is to study the SZ signal in a large sample of galaxy clusters by combining signals from known X-ray clusters. Therefore, we first assemble X-ray cluster catalog by searching the X-ray Galaxy Clusters Database (BAX)¹. The database provides a comprehensive compilation of cluster properties from the literature, including the position on the sky, redshift, and X-ray measurements such as luminosity and/or temperature. The first pass in our cluster selection requires that clusters have measured X-ray temperature. We further remove clusters with multiple entries in the database, and those that lie too close to each other in projection. Although the resulting sample

¹ <http://bax.ast.obs-mip.fr/>

is not based on any statistically complete selection, we attempt to make the temperature measurements as consistent as possible, by adopting the ones that do not include the central regions of the clusters, or those obtained through a two-temperature component analysis, thus minimizing effect of any “cool core” (CC) in the cluster mass determination. Preference is given to a few studies that provide such temperature measurement for large samples of clusters (Finoguenov et al. 2001; Fukazawa et al. 2004; Ikebe et al. 2002). While in the former two studies, the central regions have been excised, in the latter, the temperature is given by the hotter component of their two-temperature model. This leaves us with a sample of 260 clusters with measured X-ray temperatures (Fig. 1).

For a fraction of our final cluster sample, estimates of the ICM gas cooling time in the cluster central region are available in the literature (White et al. 1997; Peres et al. 1998; Bauer et al. 2005), thus allowing an investigation of the effect of the cool core on the cluster baryon budget. Cool cores are found in $\sim 50\%$ of nearby clusters, and although they show similar scaling properties across a wide mass range, they behave very differently from the inner regions of non-CC clusters (Sanderson et al. 2006). We refer to CC clusters as those with their central cooling times more than 3σ below half of the Hubble time (7 Gyr). In particular, for a subset of our sample with $T_X > 3$ keV (and after point source contamination cut, explained in Sec. 2.2), which comprises 193 of our clusters, 80 clusters have measured central cooling times, and 39 of them are classified as cool core by this criterion.

2.2 Extracting the SZ profile

Our primary task is a measurement of the mean ICM pressure profiles by combining SZ signals from known X-ray clusters. In ALS05, we assumed a functional form for the ICM profiles to derive the pressure profile from data. In this work, we go a step further by developing a model-independent method to perform these measurements. This will help minimize systematic uncertainties due to theoretical modeling of clusters, which are often the dominant sources of uncertainties in a model-dependent SZ analysis.

The idea is based on the fact that clusters are expected to be self-similar and exhibit universal dark matter (NFW, Navarro et al. 1997) as well as ICM profiles (Komatsu & Seljak 2001; Ostriker et al. 2005). Recent cosmological cluster simulations support that the ICM pressure profiles in cluster outskirt is remarkably self-similar, even in the presence of gas cooling and star formation (da Silva et al. 2004; Motl et al. 2005; Nagai 2006). Since the self-similar cluster forms a one-parameter family of the ICM pressure profile, both the radial extent and the amplitude of these profiles can be scaled by a single parameter, which can be chosen to be the total mass, X-ray or virial temperature of the cluster.

The key ingredient of our method is to use the observed X-ray temperature of clusters to set the expected extent of the ICM profile, and use the WMAP maps to find the mean normalization. We use a simple analytic ICM model to set this scale:

$$r_{200} = (1.16 \text{ Mpc}) \left(\frac{H(z)}{100 \text{ km/s/Mpc}} \right)^{-1} \left(\frac{T_X}{5 \text{ keV}} \right)^{1/2}, \quad (1)$$

where r_{200} is the radius of the sphere within which the mean density of the cluster is 200 times the critical density of the Universe, $\rho_{\text{crit}} = 3H^2(z)/(8\pi G)$, $H(z)$ is the Hubble constant at the redshift of the cluster, and T_X is the observed X-ray temperature of the cluster. Following ALS05, the model is based on a spherically symmetric NFW gravitational potential with concentration $c_{200} = 5$, and a polytropic ICM in hydrostatic equilibrium. Note that, for a cluster of a given T_X , Eq. 1 provides r_{200} that agrees with the best fit scaling relation of the recent *Chandra* observation of X-ray clusters (Vikhlinin et al. 2006) with the accuracy better than 5% level².

Once the profiles are scaled at r_{200} , we search for the SZ signal out to $4r_{200}$ radius, since the shock heated gas is only expected to be present within a few times the virial radius of the clusters. Given that the CMB signal is correlated on the degree scale (Doppler peak) in the sky, it is important to distinguish between primary CMB and SZ signal, and also account for WMAP beam smearing. Therefore, we include pixels out to $8\theta_{200} + 2$ deg, where θ_{200} is the angular size of r_{200} in the sky³. We then aim to constrain spherically averaged pressure profiles within radial bins that are logarithmically spaced in radius, and are centered at 0.25, 0.5, 1, 2, and $4r_{200}$. We assume that pressure is smoothly interpolated as $P_{\text{gas}}(r) = A + Br^{-3}$ in between the centers of the bins, where A and B are constants, and r^{-3} behavior is motivated by the dark matter/gas/pressure profile in the outskirts of simulated haloes (see Fig. 2). For completeness, we further assume $P_{\text{gas}}(r) \propto r^{-2}$ within $0.25r_{200}$ of the cluster center.

The dominant sources of noise for our SZ measurement on angles that can be resolved by WMAP experiment are WMAP detector noise and CMB primary anisotropies, which are both expected to be Gaussian to a good approximation. Therefore, minimizing

$$\chi^2 = \sum_{i,j;a,b} [T_{ia} - S_{ia}] C_{ia,jb}^{-1} [T_{jb} - S_{jb}], \quad (2)$$

is the optimum method of constraining the cluster SZ profile, S_{ia} (which is a superposition of our radial pressure bins), from the observed CMB temperature maps T_{ia} . Here i and j sum over WMAP pixels, while a and b sum over WMAP frequency bands, Q(41 GHz), V(61 GHz), W(94 GHz). The noise covariance matrix $C_{ia,jb}$ is the sum of primary CMB correlation function (using CAMB⁴; Lewis et al. 2000), which dominates on large pixel separations, and the WMAP detector noise which is assumed to be uncorrelated

² However, Nagai et al. (2007) find that the estimated r_{200} from hydrostatic equilibrium is biased low (by about 10%) on average, if subsonic turbulent gas motions are present and their pressure contribution is not explicitly accounted for (also see Rasia et al. 2006). In Sec. 4.2, we discuss the implications of using a higher normalization for the $r_{200} - T_X$ relation.

³ For example, for a small cluster, in order to find the SZ profile, the mean (large angle) primary CMB background needs to be subtracted. Including pixels beyond the cluster helps with setting this background.

⁴ <http://camb.info/>

for different pixels/frequencies. Note that both $C_{ia,jb}$ and S_{ia} need to be convolved with detector beam+pixel window functions. For WMAP, the effective beam radii range from 0.3 deg for Q-band to 0.1 deg for W band, while we use WMAP foreground cleaned maps in $N_{side} = 512$ HEALPix format (Górski et al. 2005; $(0.1 \text{ deg})^2$ pixels). We mask out all the pixels within Kp2 Galactic mask ($\sim 13\%$ of the sky), but do not mask out the point sources, as they are correlated with the clusters in our sample. In order to deal with a tractable covariance matrix, we progressively degrade the map pixel resolution towards the cluster outskirts, so that we have $\lesssim 800$ pixels per cluster. Moreover, in order to account for the uncertainty in measured T_X , as well as a 15% intrinsic scatter in the $r_{200} - T_X$ relation (seen in our simulated clusters; see Sec. 2.3), we divide the χ^2 for each cluster by a constant factor.

Point sources are additional sources of contamination of the SZ signal. The contamination is expected to be the largest in the lowest frequencies. So, to minimize the contamination, we first exclude any cluster that contains a radial bin with larger than $+3\sigma$ Q-band signal⁵ (remember that SZ signal is negative for WMAP frequencies). This excludes 18 of our clusters, only 5 of which have $T_X > 3 \text{ keV}$. Additionally, we assume a radio point source with a flat spectrum, which is shown to be consistent with the spectrum of point sources observed by WMAP (Bennett et al. 2003a), at the center of each cluster. Note, however, that our results remain virtually unchanged even if we use a steeper spectrum obtained in Coble et al. (2006) for fainter cluster radio sources. To find the ICM pressure profile, we then marginalize over the mean amplitude of the central source, as well as a mean point source contamination of the innermost radial bin, which are expected to be the dominant sources of contamination of the SZ signal.

2.3 Hydrodynamic Simulations

In this study, we use high-resolution cosmological simulations of nine hot ($T_X > 3 \text{ keV}$), massive galaxy clusters forming in the flat ΛCDM model: $\Omega_m = 1 - \Omega_\Lambda = 0.3$, $\Omega_b = 0.04286$, $h = 0.7$ and $\sigma_8 = 0.9$, where the Hubble constant is defined as $100h \text{ km s}^{-1} \text{ Mpc}^{-1}$, and σ_8 is the power spectrum normalization on $8h^{-1} \text{ Mpc}$ scale. The simulations follow dissipationless dark matter and stars, as well as dissipative gas dynamics, and include a number of physical processes critical to galaxy formation, including radiative cooling, star formation, stellar feedback and metal enrichment. The simulations were performed with the Adaptive Refinement Tree (ART) N -body+gas dynamics code (Kravtsov 1999; Kravtsov et al. 2002), an Eulerian code that uses adaptive mesh refinement to greatly increase the resolution in the high density region and resolve formation and evolution of cluster galaxies and their impact on cluster gas. Massive clusters with $T_X > 3.7 \text{ keV}$, for example, are simulated in a box size of 120 Mpc with the spatial resolution of $3.5 h^{-1} \text{kpc}$ and the mass resolution of $9 \times 10^8 h^{-1} M_\odot$. Less massive clusters are simulated in a smaller box of 80 Mpc in size with higher spatial ($\approx 2.5 h^{-1} \text{kpc}$) and mass

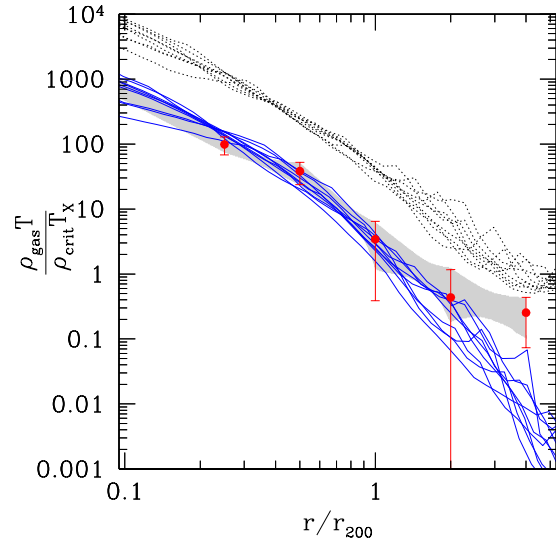


Figure 2. Mean pressure profile of 193 of our most massive clusters with $T_X > 3 \text{ keV}$ (points+errorbars). The gray area shows the 68% region allowed by this measurement, assuming $P_{\text{gas}} > 0$ prior, which reflect the errors, as well as their correlations. The blue/solid curves are predicted pressure profiles from nine simulated clusters with $T_X > 3 \text{ keV}$, while black/dotted curves show dark matter density from the same simulations, divided by the critical density of the Universe.

$(3 \times 10^8 h^{-1} M_\odot)$ resolutions. Throughout this work, we use two different average temperatures of simulated clusters. The first is a X-ray spectral temperature, T_X , a value derived from a single-temperature fit to the integrated cluster spectrum within r_{500} extracted from the mock Chandra images excluding the core ($r < 0.15r_{500}$) and detectable small-scale clumps (Nagai et al. 2007). We also compute a gas-mass-weighted temperature, denoted as $\langle T \rangle$ throughout this paper, obtained by weighting of the 3D temperature with the gas density measured directly in simulations. Note that $\langle T \rangle_{200}$ is the gas-mass-weighted average temperature measured within r_{200} . These simulations have been used to study the effects of galaxy formation on the Sunyaev-Zel'dovich effect (Nagai 2006) and the baryon fraction in clusters (Kravtsov et al. 2005). These studies are based on a sample of 11 simulated clusters with only 4 clusters massive enough to be included in the current study. Since then, we have simulated five more massive clusters, making the total sample of 16 clusters, from which we select nine massive clusters with $T_X > 3 \text{ keV}$ for the current study. The detailed description and our cluster sample are described in (Nagai et al. 2007).

Note that, in order to compare simulations with observations, the simulated gas density or pressure is normalized by the ratio of cosmic concordance baryonic mass fraction ($= \Omega_b/\Omega_m = 0.168 \pm 0.007$; Spergel et al. 2006) to the value used in the simulations.

⁵ Note that the systematic bias in the mean due to a 3σ truncation of a Gaussian probability function is less than 0.005σ .

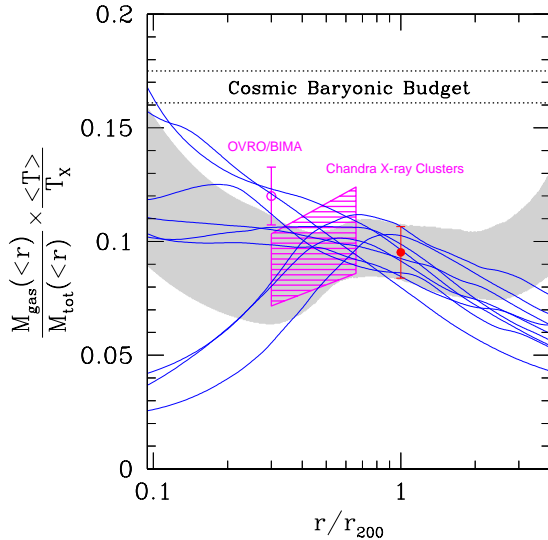


Figure 3. The ratio of total thermal energy to the mass times T_X , for the same clusters as in Fig. 2. The colors are the same as in Fig. 2, and we integrate over the pressure profiles to find total energy, $M_{\text{gas}}\langle T \rangle(r)$, enclosed within radius r , while we estimate the total mass from an NFW profile. The dotted lines show the total cosmic baryonic budget of 0.168 ± 0.007 (Spergel et al. 2006). The dashed region shows the Chandra observational constraints from 8 X-ray clusters (Vikhlinin et al. 2006), while the open point+errorbar is the most recent SZ constraint from OVRO/BIMA interferometers (LaRoque et al. 2006).

3 OBSERVATIONAL RESULTS

3.1 Universal Pressure Profile

The main result of our analysis is shown in Fig. 2. It shows the mean ICM pressure profile ($P \equiv \rho_{\text{gas}}T$), normalized to the critical density of the Universe at the cluster's redshift times its observed X-ray temperature ($\rho_{\text{crit}}T_X$). In this plot, we only include clusters with $T_X > 3$ keV (or $M_{200} \gtrsim 2.4 \times 10^{14} M_\odot$). The points+errorbars show our best fit measurement for a universal pressure profile. The gray area shows the 68% region allowed by this measurement, assuming $P_{\text{gas}} > 0$ prior, which reflect the errors, as well as their correlations. The best fit measurement of Fig. 2 is preferred to null at $\Delta\chi^2 = 47$. The simulated profiles can improve χ^2 by 31–43, which implies a 6–7 σ confirmation of the simulated models, with respect to null.

Our measurements of the mean ICM pressure profiles closely match the numerical prediction for the pressure profiles of nine simulated clusters (indicated by blue/solid lines) in the same temperature range. It is also interesting to notice the similarity of the observed ICM pressure and the simulated dark matter density profiles, indicated by black/dotted lines.

3.2 Total Thermal Energy of the Cluster

In Fig. (3), we examine the integrated pressure, or equivalently thermal energy of the ICM as a function of cluster centric radius in units of r_{200} . Here we normalize the thermal energy ($M_{\text{gas},200}\langle T \rangle_{200}$) to the total mass of the cluster (ex-

pected from an NFW profile with $c_{200} = 5$) times the cluster X-ray temperature ($M_{\text{tot},200}T_X$). The solid point+errorbar shows the mean and standard deviation of this quantity at r_{200} , and thus corresponds to our measurement of the mean ICM thermal energy:

$$\left(\frac{M_{\text{gas},200}}{M_{\text{tot},200}} \right) \left(\frac{\langle T \rangle_{200}}{T_X} \right)_{\text{WMAP}} = 0.095 \pm 0.011. \quad (3)$$

The results is in very good agreement with our simulated clusters:⁶

$$\left(\frac{M_{\text{gas},200}}{M_{\text{tot},200}} \right) \left(\frac{\langle T \rangle_{200}}{T_X} \right)_{\text{Sim.}} = 0.093 \pm 0.003, \quad (4)$$

which are shown by thick curves in Fig. 3. Finally, the dashed region shows the most detailed available X-ray study of 8 clusters (Vikhlinin et al. 2006) ($T_X > 3$ keV), observed by Chandra X-ray observatory, while the open dot with the errorbar shows the constraints from SZ observations of 38 massive clusters with OVRO/BIMA interferometers (LaRoque et al. 2006). Both of these studies are also fully consistent with our SZ measurements from the WMAP 3 year data.

Knowing $\langle T \rangle_{200}/T_X$, we can convert the thermal energy fraction into the gas fraction of clusters. For our nine simulated clusters with $T_X > 3$ keV, we estimate that the ratio of mean to X-ray estimated temperature is $\langle T \rangle_{200}/T_X = 0.87 \pm 0.02$. Using this value, the cluster gas fraction is

$$\left(\frac{M_{\text{gas},200}}{M_{\text{tot},200}} \right)_{\text{WMAP}} = 0.109 \pm 0.013 \quad (5)$$

for the WMAP data. The value is significantly smaller than the cosmic baryon fraction of $\Omega_b/\Omega_m = 0.168 \pm 0.007$ (Spergel et al. 2006). If the clusters contain a representative mix of dark matter and baryons of the Universe ($M_{\text{baryons}}/M_{\text{tot}} \approx \Omega_b/\Omega_m$), our results indicate that a fraction

$$\frac{M_{\text{missing}}}{M_{\text{baryons}}} = \frac{M_{\text{baryons}} - M_{\text{gas}}}{M_{\text{baryons}}} = 0.35 \pm 0.08 \quad (6)$$

of the cluster baryons are missing from the hot ICM. As we discuss more in § 4.3, this number is far too large to be accounted for by the observed stellar and cold gas fraction of $\approx 10\%$ in our T_X range (Gonzalez et al. 2005; Lin & Mohr 2004). These results are in agreement with our earlier analysis by ALS05.

3.3 Systematic Trends with T_X

Exploiting a large coverage of cluster X-ray temperatures and masses, it would be interesting to study if there is any systematic trend in the gas fraction as a function of T_X . Fig. 4 shows the thermal energy to mass ratio within r_{200} as a function T_X , where we have binned clusters into 2 keV temperature bins. The number of clusters in each bin, from left to right is 44, 66, 84, 41, 16, and 9. Here again, we see that our SZ measurements are consistent with predictions from hydrodynamic simulations (open stars), as well as our

⁶ The quoted error is the sample variance error of the mean energy fraction for the simulated clusters with $T_X > 3$ keV.

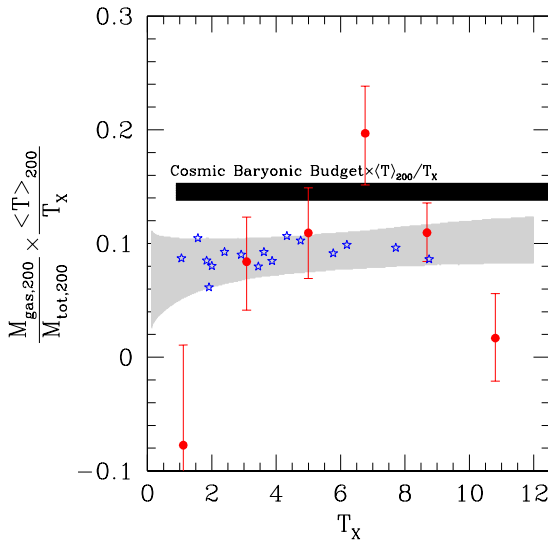


Figure 4. Thermal energy to mass times T_X ratio as a function of T_X . Solid points+errorbars show the measured total thermal energy to mass ratio within r_{200} for all our clusters, binned within $\Delta T_X = 2$ keV bins. Open stars show the same ratio for our hydrodynamic simulations, while the gray area shows the 68% uncertainty range of the best power law fit to our data (Eq. 7). The black horizontal bar shows the total cosmic baryonic budget (Spergel et al. 2006), multiplied by the mean temperature correction from the simulations.

earlier analysis (ALS05). The best fit power law to our measurement points (weighted by their errors) is

$$\left(\frac{M_{\text{gas},200}}{M_{\text{tot},200}} \right) \left(\frac{\langle T \rangle_{200}}{T_X} \right) = (0.098 \pm 0.015) \left(\frac{T_X}{6.4 \text{ keV}} \right)^{0.15 \pm 0.18}, \quad (7)$$

which is represented by the gray area in Fig. 4, and does not show any significant monotonic trend throughout the T_X range, a trend similar to the simulated clusters.

The measurement points in Fig. 4 have almost a factor of two more scatter than is expected from the measurement errors. This could be caused by a possible systematic underestimate of our measurement errors, or otherwise by an intrinsic scatter in the ICM properties of different clusters. An important clue to the reason behind this scatter, as well as the nature of missing baryons may come from looking at a sub-sample of our clusters with resolved cool cores (39 CC-clusters with $T_X > 3$ keV; see Sec. 2.1). The energy fraction of the CC-clusters is

$$\left(\frac{M_{\text{gas},200}}{M_{\text{tot},200}} \right) \left(\frac{\langle T \rangle_{200}}{T_X} \right)_{\text{CC}} = 0.142 \pm 0.019, \quad (8)$$

which is significantly larger than the main sample, and is consistent with no missing baryons after the correction for $\langle T \rangle_{200}/T_X$. Moreover, the pressure profile seems significantly flatter than the simulated profiles within $0.5r_{200}$. Although the fact that the ICM gas fraction is systematically higher for cool core clusters in Eq. 8 may signal an unknown systematic problem with our method of subtracting point sources, it may also be caused by a real anti-correlation between the missing baryons and the central cooling activity. Further observational studies are clearly needed to resolve these issues.

Although our sample includes X-ray clusters with measured temperatures out to redshift 1, less than 20% of the statistical significance of our SZ detection in our sample comes from clusters with $z > 0.2$. This is because the virial radius of clusters (~ 1.5 Mpc) at $z \gtrsim 0.2$ falls below the WMAP detector beam size of ~ 0.2 deg. Therefore, it would be difficult to study any redshift evolution in our sample, and thus it will not be explored here.

4 DISCUSSIONS

4.1 Comparison with our previous analysis

One may wonder why, despite the use of the 3 year WMAP maps as well as more X-ray clusters, the significance of our SZ detection has not significantly increased compared to our previous analysis with the 1st year WMAP maps in ALS05. This is mainly due to the fact that, in our new analysis we parameterize the mean cluster signal by 8 free parameters (6 for pressure profile, and 2 for point sources), while our previous analysis only used 2 (1 for the total gas fraction, and 1 for the over all point source contamination). Therefore, the error on the individual parameters, such as the total gas fraction, is increased due to the extra marginalizations involved in the analysis.

Despite the use of a completely different method, our main conclusion: a fraction of 30% – 40% missing ICM baryons, has not changed from ALS05. However, we did not find any systematic T_X dependence in the energy fraction in Eq. 7. This shows a $\sim 2\sigma$ discrepancy with our earlier analysis of WMAP SZ signal, where we found an almost linear dependence on T_X . However, our earlier analysis assumed a universal pressure profile for all clusters. Therefore, one way to reconcile the two analyses is for the profiles to be systematically shallower for clusters with $T_X \lesssim 4$ keV, which is indeed seen in our sample, but it is difficult to quantify due to the low significance of SZ signal in cooler clusters.

4.2 Systematic and Theoretical Uncertainties

One of the main improvements from our previous analysis in ALS05 is the use of a model-independent method to derive the mean ICM profiles from the WMAP 3yr data. This will help minimize systematic errors arising from uncertainties in theoretical modeling, which often dominate systematic uncertainties of the analyses carried out using a model-dependent method.

The only theoretical assumption in our derivation of the mean ICM pressure profile has been the use of Eq. 1 to infer the cluster masses or radii based on their measured X-ray temperatures. Therefore, any systematic errors in this scaling relation translate into an error in the cluster total mass estimate, which could bias our estimate of the cluster gas mass fractions. Indeed, the normalization of the $r_{200} - T_X$ used in our analysis is consistent with hydrostatic estimates from X-ray observations (Vikhlinin et al. 2006), which are about 10% smaller than the simulated normalization (Kravtsov et al. 2006). However, even if there is a systematic error in the normalization of $r_{200} - T_X$ relation, Eq. 1 can be viewed as the definition of r_{200} in terms of the observed cluster X-ray temperature, which simply defines a

unified radial unit for the mean pressure profile. In other words, the bias, if present, results in the re-definition (or re-scaling) of r_{200} . In this way, our measurements of mean pressure profile is indeed *model-independent*. However, any inference about the missing ICM baryonic fraction would be affected by a systematic error in our assumed $r_{200} - T_X$ relation. For example, using the higher normalization (inferred from simulations) can boost the missing baryon fraction to $\sim 50\%$.

4.3 Missing Baryons or New Astrophysics?

The most puzzling result of our analysis is that a significant fraction ($35\% \pm 8\%$) of the baryons are missing from the ICM. On average, the fraction of the observed stellar mass associated with galaxies in clusters within our T_X range is less than 10% (Lin et al. 2003), leaving room for an unaccounted baryonic component of $25 \pm 8\%$. Although the evidence for this component is marginal (3.1σ) from our analysis, independent verification from other SZ and X-ray observations (LaRoque et al. 2006; Ettori 2003; Vikhlinin et al. 2006, see Fig. 3) strongly support the case for a missing component of cluster baryons.

Interestingly, modern cosmological cluster simulations that include gas cooling and star formation also give the ICM mass fraction very similar to the observed values (Kravtsov et al. 2007). The good agreement in the ICM mass fraction between simulations and observations suggests that the simulations reproduce the hot ICM of the real clusters reasonably well (Nagai et al. 2007). However, the agreement is achieved while the stellar fractions within r_{500} of the simulated clusters are a factor of two to three greater than the observed stellar fraction.

This raises a possibility that a significant fraction of baryonic mass may be hidden in a form that is difficult to detect with ordinary observational means. One such example is diffuse intracluster light (ICL), which would be challenging to detect observationally, but could potentially hide significant amount of stellar mass in the vast intracluster space. The measurements of ICL are now becoming possible with very deep photometry. Although the measurements are quite challenging, a number of ICL observations indicate that no more than 10-50% of stars could be found in the form of ICL (Lin & Mohr 2004; Zibetti et al. 2005; Gonzalez et al. 2005; Monaco et al. 2006). Similar results are also obtained in cosmological cluster simulations (Murante et al. 2004; Sommer-Larsen et al. 2005). Alternatively, one may also envisage hiding baryons in a form of cold and compact dark baryonic clouds formed from local cooling instabilities within ICM (or proto-ICM), similar to the high velocity clouds in the local group. At the moment, there is essentially no constraint on such clouds as long as their temperature is below 10 K, and/or their covering fraction of the cluster radio map is less than unity (Dwarakanath et al. 1994).

It has been suggested that a soft X-ray excess in observations of X-ray clusters can be interpreted as evidence for a warm (~ 0.1 keV) compact phase of the ICM, which would not contribute to the SZ signal, while containing a significant fraction of the ICM baryons (e.g., Bonamente et al. 2005, and references therein). However, the extragalactic nature of the soft X-ray excess is still controversial

(e.g., Bregman & Lloyd-Davies 2006). Moreover, it is not clear how the strong cooling instability of any such component could be avoided in the cluster environment.

Yet another possibility that has been recently proposed by Loeb (2007), is thermal diffusion or evaporation of baryons out of the virial radius of the cluster. The thermal evaporation, if efficient, can remove the gas out of the virial radius, bringing the cluster gas fraction down without creating stars (but see Medvedev 2007). Similarly, inclusion of diffusive processes in hydrodynamical simulations may on one hand suppress cooling (Zakamska & Narayan 2003), thus bringing down the cool gas fraction into better agreement with the observed stellar content, while on the other hand remove the thermal energy of the ICM out of the virial radius (Loeb 2002), explaining the low gas fractions inferred from our SZ observations. However, recent numerical simulations that included (some of) these processes suggest that they cannot affect the overcooling problem significantly (Dolag et al. 2004).

5 SUMMARY AND FUTURE PROSPECTS

We report a 9σ detection of the SZ signal in the CMB maps of WMAP 3yr data, through study of a sample of 193 massive clusters with observed X-ray temperatures larger than 3 keV. The improvements from the previous analyses in ALS05 are in both data and analysis methods: (1) the use of the WMAP 3yr data release (Hinshaw et al. 2006) and (2) the use of a model-independent method to measure the mean ICM pressure profile to minimize systematic uncertainties due to theoretical modeling.

The resulting pressure profile is in good agreement with measurements of recent X-ray and SZ observations as well as hydrodynamical cluster simulations. Our result indicates that $35 \pm 8\%$ of the baryons are missing from the ICM, which is significantly larger than the observed stellar or cold gas fraction of about 10% so far accounted for in clusters. The evidence for this component is marginal (3.1σ) from our analysis, but independent verification from other SZ (LaRoque et al. 2006) and X-ray observations (Ettori 2003; Vikhlinin et al. 2006) strongly support the case for a missing component of cluster baryons. This signals the presence of a missing baryonic component or yet-unknown astrophysical processes that could lower the cluster baryon fraction.

The problem of missing thermal energy of the ICM introduces a new puzzle into the standard cluster formation scenario. Further investigations of the ICM physics are thus essential for our understanding of cluster formation as well as applications of cluster-based cosmological tests using X-ray and SZ cluster surveys. On the theoretical front, it is important to understand details and relative importance of gas cooling and heating by supernovae (SN) and active galactic nuclei (AGN) and their effects on the ICM properties. Further numerical investigations of diffusive processes are also critical for understanding of cluster plasma phenomena. Observationally, it is important to further refine measurements of X-ray, SZ, lensing and optical/IR observations and consolidate the measurements of the cluster baryon budgets in clusters. Large microwave interferometer arrays such as

ALMA⁷ will ultimately be able to map the ICM pressure profile in the outskirts of individual clusters with exquisite accuracy (Kocsis et al. 2005), while the next generation of high-resolution, multi-frequency CMB experiments, such as APEX, ACT, SPT, and SZA⁸, will be able to probe the thermal energy content to high redshifts, opening new windows for the future studies of structure formation and cosmology.

ACKNOWLEDGMENTS

We would like to thank Jacqueline van Gorkom, Andrey Kravtsov, Adam Lidz, Avi Loeb, Ramesh Narayan, and Jerry Ostriker for helpful comments and discussions. YTL acknowledges support from NSF PIRE grant OISE-0530095 and FONDAP-Andes. DN is supported by the Sherman Fairchild Postdoctoral Fellowship at CalTech. AJRS acknowledges support by PPARC.

The analysis presented in this paper have made use of the HEALPix package (Górski et al. 2005, <http://healpix.jpl.nasa.gov/>), the X-Ray Galaxy Clusters Database (BAX; <http://bax.ast.obs-mip.fr/>), and the Legacy Archive for Microwave Background Data Analysis (LAMBDA; <http://lambda.gsfc.nasa.gov/>).

REFERENCES

Afshordi N., Lin Y.-T., Sanderson A. J. R., 2005, *ApJ*, 629, 1, ADS, astro-ph/0408560

Afshordi N., Loh Y.-S., Strauss M. A., 2004, *Phys. Rev. D*, 69, 083524, ADS, astro-ph/0308260

Bauer F. E., Fabian A. C., Sanders J. S., Allen S. W., Johnstone R. M., 2005, *MNRAS*, 359, 1481, ADS, astro-ph/0503232

Bennett C. L., et al., 2003a, *ApJS*, 148, 97, astro-ph/0302208

Bennett C. L., et al., 2003b, *ApJS*, 148, 1, ADS, astro-ph/0302207

Bialek J. J., Evrard A. E., Mohr J. J., 2001, *ApJ*, 555, 597, ADS, astro-ph/0010584

Birkinshaw M., 1999, *Phys. Rep.*, 310, 97, ADS, astro-ph/9808050

Bonamente M., Lieu R., Mittaz J. P. D., Kaastra J. S., Nevalainen J., 2005, *ApJ*, 629, 192, ADS, astro-ph/0504092

Borgani S., 2006, ArXiv Astrophysics e-prints, astro-ph/0605575

Bregman J. N., Lloyd-Davies E. J., 2006, *ApJ*, 644, 167, ADS, astro-ph/0602527

Carlstrom J. E., Holder G. P., Reese E. D., 2002, *ARA&A*, 40, 643, ADS, astro-ph/0208192

Coble K., Carlstrom J. E., Bonamente M., Dawson K., Holzapfel W., Joy M., LaRoque S., Reese E. D., 2006, ArXiv Astrophysics e-prints, astro-ph/0608274

da Silva A. C., Kay S. T., Liddle A. R., Thomas P. A., 2004, *MNRAS*, 348, 1401, astro-ph/0308074

Dolag K., Jubelgas M., Springel V., Borgani S., Rasia E., 2004, *ApJ*, 606, L97, astro-ph/0401470

Dwarakanath K. S., van Gorkom J. H., Owen F. N., 1994, *ApJ*, 432, 469, ADS

Eke V. R., Navarro J. F., Frenk C. S., 1998, *ApJ*, 503, 569, ADS, astro-ph/9708070

Ettori S., 2003, *MNRAS*, 344, L13, ADS, astro-ph/0305296

Ettori S., Dolag K., Borgani S., Murante G., 2006, *MNRAS*, 365, 1021, astro-ph/0509024

Evrard A. E., 1990, *ApJ*, 363, 349, ADS

Finoguenov A., Reiprich T. H., Böhringer H., 2001, *A&A*, 368, 749, astro-ph/0010190

Fosalba P., Gaztañaga E., 2004, *MNRAS*, 350, L37, astro-ph/0305468

Fosalba P., Gaztañaga E., Castander F. J., 2003, *ApJ*, 597, L89, astro-ph/0307249

Frenk C. S., et al., 1999, *ApJ*, 525, 554, astro-ph/9906160

Fukazawa Y., Makishima K., Ohashi T., 2004, *PASJ*, 56, 965, astro-ph/0411745

Geisbuesch J., Hobson M., 2006, ArXiv Astrophysics e-prints, ADS, astro-ph/0611567

Gonzalez A. H., Zabludoff A. I., Zaritsky D., 2005, *ApJ*, 618, 195, ADS, astro-ph/0406244

Górski K. M., Hivon E., Banday A. J., Wandelt B. D., Hansen F. K., Reinecke M., Bartelmann M., 2005, *ApJ*, 622, 759, astro-ph/0409513

Hernández-Monteagudo C., Rubiño-Martín J. A., 2004, *MNRAS*, 347, 403, astro-ph/0305606

Hinshaw G., et al., 2006, ArXiv Astrophysics e-prints, ADS, astro-ph/0603451

Ikebe Y., Reiprich T. H., Böhringer H., Tanaka Y., Kitayama T., 2002, *A&A*, 383, 773, astro-ph/0112315

Jarosik N., et al., 2006, ArXiv Astrophysics e-prints, ADS, astro-ph/0603452

Kocsis B., Haiman Z., Frei Z., 2005, *ApJ*, 623, 632, ADS, astro-ph/0409430

Komatsu E., Seljak U., 2001, *MNRAS*, 327, 1353, ADS, astro-ph/0106151

Kravtsov A. V., 1999, PhD thesis, New Mexico State University

Kravtsov A. V., Klypin A., Hoffman Y., 2002, *ApJ*, 571, 563, astro-ph/0109077

Kravtsov A. V., Nagai D., Vikhlinin A. A., 2005, *ApJ*, 625, 588, astro-ph/0501227

Kravtsov A. V., Nagai D., Vikhlinin A. A., 2007, *ApJ*, in preparation

Kravtsov A. V., Vikhlinin A., Nagai D., 2006, *ApJ*, 650, 128, ADS, astro-ph/0603205

LaRoque S. J., Bonamente M., Carlstrom J. E., Joy M. K., Nagai D., Reese E. D., Dawson K. S., 2006, *ApJ*, 652, 917, ADS, astro-ph/0604039

Lewis A., Challinor A., Lasenby A., 2000, *ApJ*, 538, 473, astro-ph/9911177

Lieu R., Mittaz J. P. D., Zhang S.-N., 2006, *ApJ*, 648, 176, ADS, astro-ph/0510160

Lin Y.-T., Mohr J. J., 2004, *ApJ*, 617, 879, astro-ph/0408557

Lin Y.-T., Mohr J. J., Stanford S. A., 2003, *ApJ*, 591, 749, astro-ph/0304033

Loeb A., 2002, *New Astronomy*, 7, 279, astro-ph/0203450

Loeb A., 2007, *Journal of Cosmology and Astro-Particle Physics*, 3, 1, ADS, astro-ph/0606572

⁷ <http://www.almajrao.edu/>

⁸ <http://bolo.berkeley.edu/apexsz/>;

<http://www.physics.princeton.edu/act/>;

<http://spt.uchicago.edu/>; <http://astro.uchicago.edu/sza/>

Lubin L. M., Cen R., Bahcall N. A., Ostriker J. P., 1996, ApJ, 460, 10, ADS, astro-ph/9509148

McCarthy I. G., Bower R. G., Balogh M. L., 2006, ArXiv Astrophysics e-prints, astro-ph/0609314

Medvedev M. V., 2007, ArXiv Astrophysics e-prints, ADS, astro-ph/0702356

Metzler C. A., Evrard A. E., 1994, ApJ, 437, 564, ADS, astro-ph/9309050

Mohr J. J., Mathiesen B., Evrard A. E., 1999, ApJ, 517, 627, ADS, astro-ph/9901281

Monaco P., Murante G., Borgani S., Fontanot F., 2006, ApJ, 652, L89, astro-ph/0610045

Motl P. M., Hallman E. J., Burns J. O., Norman M. L., 2005, ApJ, 623, L63, astro-ph/0502226

Murante G., Arnaboldi M., Gerhard O., Borgani S., Cheng L. M., Diaferio A., Dolag K., Moscardini L., Tormen G., Tornatore L., Tozzi P., 2004, ApJ, 607, L83, astro-ph/0404025

Myers A. D., Shanks T., Outram P. J., Frith W. J., Wolfendale A. W., 2004, MNRAS, 347, L67, astro-ph/0306180

Nagai D., 2006, ApJ, 650, 538, astro-ph/0512208

Nagai D., Kravtsov A. V., Vikhlinin A., 2007, ApJ, in preparation

Nagai D., Vikhlinin A., Kravtsov A. V., 2007, ApJ, 655, 98, ADS, astro-ph/0609247

Navarro J. F., Frenk C. S., White S. D. M., 1995, MNRAS, 275, 720, ADS, astro-ph/9408069

Navarro J. F., Frenk C. S., White S. D. M., 1997, ApJ, 490, 493, ADS, astro-ph/9611107

Ostriker J. P., Bode P., Babul A., 2005, ApJ, 634, 964, astro-ph/0504334

Peres C. B., Fabian A. C., Edge A. C., Allen S. W., Johnstone R. M., White D. A., 1998, MNRAS, 298, 416, astro-ph/9805122

Rasia E., Ettori S., Moscardini L., Mazzotta P., Borgani S., Dolag K., Tormen G., Cheng L. M., Diaferio A., 2006, MNRAS, 369, 2013, astro-ph/0602434

Sanderson A. J. R., Ponman T. J., O'Sullivan E., 2006, MNRAS, 372, 1496, astro-ph/0608423

Schmidt R. W., Allen S. W., Fabian A. C., 2004, MNRAS, 352, 1413, ADS, astro-ph/0405374

Sommer-Larsen J., Romeo A. D., Portinari L., 2005, MNRAS, 357, 478, ADS, astro-ph/0403282

Spergel D. N., et al., 2006, ArXiv Astrophysics e-prints, ADS, astro-ph/0603449

Sunyaev R. A., Zel'dovich Y. B., 1972, Comments on Astrophysics and Space Physics, 4, 173, ADS

Vikhlinin A., et al., 2006, ApJ, 640, 691, ADS, astro-ph/0507092

Vikhlinin A., Forman W., Jones C., 1999, ApJ, 525, 47, ADS, astro-ph/9905200

Voit G. M., 2005, Reviews of Modern Physics, 77, 207, ADS, astro-ph/0410173

White D. A., Jones C., Forman W., 1997, MNRAS, 292, 419, astro-ph/9707269

Zakamska N. L., Narayan R., 2003, ApJ, 582, 162, astro-ph/0207127

Zibetti S., White S. D. M., Schneider D. P., Brinkmann J., 2005, MNRAS, 358, 949, ADS, astro-ph/0501194